Published in final edited form as:
Ophthalmol Clin North Am. 2004 March ; 17(1): 7–20.

Anterior segment imaging: ultrasound biomicroscopy

Hiroshi Ishikawa, MD* and **Joel S. Schuman, MD**
UPMC Eye Center and Department of Ophthalmology, University of Pittsburgh School of Medicine, The Eye and Ear Institute, Suite 816, 203 Lothrop Street, Pittsburgh, PA 15213, USA

High-frequency ultrasound biomicroscopy (UBM) (Paradigm Medical Industries, Salt Lake City, Utah) provides high-resolution in vivo imaging of the anterior segment in a noninvasive fashion. In addition to the tissues easily seen using conventional methods (ie, slit lamp), such as the cornea, iris, and sclera, structures including the ciliary body and zonules, previously hidden from clinical observation, can be imaged and their morphology assessed. Pathophysiologic changes involving anterior segment architecture can be evaluated qualitatively and quantitatively. This article discusses the role of UBM in imaging of the anterior segment of the eye from the qualitative and quantitative analysis point of view.

Equipment and technique

The technology for UBM, originally developed by Pavlin, Sherar, and Foster, is based on 50- to 100-MHz transducers incorporated into a B-mode clinical scanner [1–3]. Higher frequency transducers provide finer resolution of more superficial structures, whereas lower frequency transducers provide greater depth of penetration with less resolution. The commercially available units operate at 50 MHz and provide lateral and axial physical resolutions of approximately 50 μm and 25 μm, respectively. Tissue penetration is approximately 4 to 5 mm. The scanner produces a 5 × 5 mm field with 256 vertical image lines (or A-scans) at a scan rate of 8 frames per second.

Each A-scan is mapped into oversampled 1024 points, with 256 gray-scale levels representing the logged amplitude of reflection, and then the number of points is downsized to 432 pixels to fit on the UBM monitor. The real-time image is displayed on a video monitor and can be recorded on videotape for later analysis. Room illumination, fixation, and accommodative effort affect anterior segment anatomy and should be held constant, particularly when quantitative information is being gathered.

The image acquisition technique has been described elsewhere and is similar to traditional immersion B-scan ultrasonography [3–5]. In the Paradigm Instruments UBM, the probe is suspended from a gantry arm to minimize motion artifacts, and lateral distortion is minimized by a linear scan format. In the OTI (Ophthalmic Technologies, Toronto, Canada) device, the probe is small and light enough not to require a suspension arm, and a sector scanning method is used. Scanning is performed with the patient in the supine position. A plastic eyecup of the appropriate size is inserted between the lids, holding methylcellulose or normal saline coupling medium. To maximize the detection of the reflected signal, the transducer should be oriented so that the scanning ultrasound beam strikes the target surface perpendicularly.

* Corresponding author. E-mail address: ishikawah@upmc.edu (H. Ishikawa).

Qualitative ultrasound biomicroscopy

The normal eye

In the normal eye, the cornea, anterior chamber, posterior chamber, iris, ciliary body, and anterior lens surface can be recognized easily (Fig. 1). The scleral spur is the only constant landmark allowing one to interpret UBM images in terms of the morphologic status of the anterior chamber angle and is the key for analyzing angle pathology. The scleral spur is located where the trabecular meshwork meets the interface line between the sclera and ciliary body.

Generally, in the normal eye, the iris has a roughly planar configuration with slight anterior bowing, and the anterior chamber angle is wide and clear. Morphologic relationships among the anterior segment structures alter in response to a variety of physiologic stimuli (ie, accommodative targets and light); therefore, maintaining a constant testing environment is critical for cross-sectional and longitudinal comparison.

Glaucoma

Angle-closure glaucoma—Iris apposition to the trabecular meshwork is the final common pathway of angle-closure glaucoma, which represents a group of disorders. This condition can be caused by one or more abnormalities in the relative or absolute sizes or positions of anterior segment structures, or by abnormal forces in the posterior segment that alter the anatomy of the anterior segment. Forces are generated to cause angle closure in four anatomic sites: the iris (pupillary block), the ciliary body (plateau iris), the lens (phacomorphic glaucoma), and behind the iris by a combination of various forces (malignant glaucoma and other posterior pushing glaucoma types). Differentiating these affected sites is the key to provide effective treatment. UBM is extremely useful for achieving this goal.

Angle occludability Examining eyes with narrow angles requires careful attention to the occludability of the angle. Although provocative testing, such as dark room gonioscopy, is useful for detecting the angle occludability, it is now rarely used, because it is subjective, time consuming, and prone to false-negative results owing to the difficulty of standardizing the slit-lamp light intensity. With UBM, dark room provocative testing can be performed in a standardized environment generating objective results by providing information on the state of the angle under normal light conditions and its tendency to occlude spontaneously under dark conditions (Fig. 2).

Pupillary block Pupillary block is the most common type of angle-closure glaucoma. At the iridolenticular contact, resistance to aqueous flow from the posterior to the anterior chamber creates an unbalanced relative pressure gradient between the two chambers, pushing the iris up toward the cornea (Fig. 3A). This abnormal resistance causes anterior iris bowing, angle narrowing, and acute or chronic angle-closure glaucoma. The other anterior segment structures and their anatomic relationships remain normal.

Laser iridectomy equalizes the pressure gradient between the anterior and posterior chambers and flattens the iris. The result is a widened anterior chamber angle (Fig. 3B).

Plateau iris A plateau iris configuration occurs owing to a large or anteriorly positioned ciliary body (pars plicata), which pushes the iris root mechanically up against the trabecular meshwork (Fig. 4). The iris root may be short and inserted anteriorly on the ciliary face, creating a narrow and crowded angle. The anterior chamber is usually of medium depth, and the iris surface looks flat or slightly convex, just like in a normal eye. With indentation gonioscopy, the “double-hump” sign is observed. The peripheral hump results from the rigid presence of the ciliary body holding the iris root; the central hump represents the center part of the iris resting over the

anterior lens surface. The space between the two humps represents the area between the ciliary processes and the endpoint of iridolenticular contact. These findings can be confirmed by performing indentation UBM (Fig. 5), a special technique that imposes mild pressure on the peripheral cornea with the skirt of a plastic eyecup so that one can simulate indentation gonioscopy [6].

Phacomorphic glaucoma Anterior subluxation of the lens may lead to angle-closure glaucoma because of the lens pushing the iris and ciliary body toward the trabecular meshwork.

Malignant glaucoma Malignant glaucoma, also known as ciliary block or aqueous misdirection, presents the greatest diagnostic and treatment challenge. Forces posterior to the lens push the lens–iris diaphragm forward, causing angle closure. UBM clearly shows that all anterior segment structures are displaced and pressed tightly against the cornea with or without fluid in the supraciliary space (Fig. 6).

Other causes of angle closure Iridociliary body cysts can produce angle-closure glaucoma. The anterior chamber angle is occluded partially or intermittently owing to singular or multiple cysts (Fig. 7). UBM is extremely useful in making the diagnosis in these cases. Other entities, such as iridociliary tumor, enlargement of the ciliary body owing to inflammation or tumor infiltration, or air or gas bubbles after intraocular surgery, may also present angle closure.

Open-angle glaucoma—The only type of open-angle glaucoma that shows characteristic findings on UBM is the pigment dispersion syndrome. In this familial autosomal dominant disease, mechanical friction between the posterior iris surface and anterior zonular bundles releases iris pigment particles into aqueous flow. These particles are deposited on structures throughout the anterior segment. The diagnostic triad consists of a Krukenberg spindle, radial transillumination defects of the midperipheral iris, and pigment deposition on the trabecular meshwork.

Typical UBM findings associated with this condition include a widely opened angle, an iris with slight concavity (bowing posteriorly), and increased iridolenticular contact (Fig. 8). As is true in pupillary block, there is a relative pressure gradient between the anterior and posterior chamber; however, because the anterior chamber is the one that holds higher pressure, this condition is called “reverse pupillary block” [7]. Laser iridotomy eliminates this pressure gradient, resulting in a flattened iris [8].

Abnormalities of the iris and ciliary body

Ultrasound biomicroscopy is helpful in differentiating solid from cystic lesions of the iris and ciliary body (see Fig. 7 and Fig. 9). The size of these lesions can be measured, and the extent to which they invade the iris root and ciliary face can be evaluated. In hypotony cases, UBM can distinguish tractional from dehiscence ciliary body detachment, which requires a different management approach [9].

Ocular trauma

Ocular trauma often limits the visibility of the ocular structure owing to the presence of hyphema. Accurate assessment of the structural damage and locating small foreign bodies can be a challenging task when clear direct visualization is not achieved. UBM can be performed over a plano soft contact lens to minimize the risk of further injury with eyecups or with infection in a micro–open wound. With the help of UBM, angle recession can be differentiated plainly from cyclodialysis [10,11].

In eyes with angle recession, the ciliary body face is torn at the iris insertion, resulting in a wide-angle appearance with no disruption of the interface in between the sclera and ciliary body (Fig. 10). In contrast, in cyclodialysis, the ciliary body is detached from its normal location at the scleral spur, creating a direct pathway from the anterior chamber to the supraciliary space (Fig. 11).

Foreign bodies generate various artifacts based on their acoustic characteristics [12]. In general, materials that contain air (ie, wood and concrete) create shadowing artifact by absorbing most of the incoming ultrasound at their sites, whereas hard and dense materials (ie, metal and glass) generate comet tail artifacts by reflecting ultrasound back and forth within the materials (Fig. 12). Scleral sutures after intraocular surgery can be identified by searching for this shadowing artifact (by refraction) (Fig. 13).

Intraocular lens position

An intraocular lens is an easy target for UBM visualization, because it is a type of foreign body. Optic and haptic locations can be assessed accurately by looking for a strong echo at their interface plane. Because the capsular bag cannot always be visualized, the most peripheral portion of the haptic defines its position in the capsular bag, ciliary sulcus, or a dislocated point (Fig. 14). This technique is used in various studies related to many different types of intraocular lenses [13–17].

Quantitative ultrasound biomicroscopy

Physical resolution and measurement precision

Physical resolution is often confused with measurement precision. Physical resolution specifies how close together two objects can be located yet still be determined to be distinct. It also specifies the smallest object detectable. Measurement precision refers to the width and height of a single pixel on the screen that can be identified by the operator using the screen cursor. The UBM measurement software calculates distance and area by counting the number of pixels along the measured line or inside the designated area and multiplies the pixel counts by the theoretical size of the pixel. Measurement precision can be better than physical resolution by over-sampling the signal.

Commercially available instruments provide lateral and axial physical resolution of approximately 50 and 25 μm, respectively. The resolution of the Paradigm device is slightly better than that of the OTI device. The theoretical lateral and axial measurement precision on the standard UBM monitor (864 × 432 pixels) is approximately 6 and 12 μm. Although UBM cannot distinguish two small objects less than 25 μm apart along the axial scanning line, it can still measure the distance between two objects far enough apart (> 25 μm, such as corneal thickness, anterior chamber depth) with 12-μm precision.

Measurement accuracy

Pavlin et al [2] reported good qualitative agreement of UBM images with histologic sections. Quantitatively, Maberly et al [18] showed good agreement by measuring the distance from the anterior margin of peripheral choroidal melanomas to the scleral spur on UBM images and histologic sections.

Pierro et al [19] compared the corneal thickness measured by UBM versus ultrasound and optical pachymetry. The UBM measurement was similar to the ultrasound pachymetry, whereas optical pachymetry showed a poor correlation with UBM and ultrasound pachymetry. Urbak [20] reported similar results. Additionally, a specially prepared plastic material was

measured with UBM and scanning electron microscopy. The axial and lateral accuracies of UBM measurements were good and reliable.

Measurement reproducibility

Tello et al [21] reported on the reproducibility of measuring Pavlin's parameters (described in detail in the next section). Intraobserver reproducibility was reasonably good, except for the angle opening distance (AOD), but interobserver reproducibility was not. Urbak et al [22,23] reported similar results. Although image acquisition differences were the major cause of this variability, the variability of the measurement process cannot be ignored.

All of Pavlin's parameters require multiple steps of measurements of a distance or an angle. The parameters are measured on the UBM monitor, allowing determination of a point-to-point distance or an angle composed of two straight lines; however, this method does not keep the previous measurement on the same screen. It is difficult and not reproducible to perform measurements that require multiple steps (ie, measuring a distance along a line drawn perpendicular to a line between the scleral spur and the corneal endothelial border that is 500 μm anterior to the scleral spur).

To minimize the variability of the measurement process, a fully automated measurement system would be ideal; however, with current technology, it would be difficult to develop such a software program. A semi-automated software system that calculates various quantitative parameters after one user input of the reference point location is a reasonable compromise. The UBM Pro 2000 (Paradigm Medical Industries, Salt Lake City, Utah) can measure the AOD in a semi-automated fashion. It has dramatically improved overall reproducibility (coefficient of variation, 7.3 to 2.5; Hiroshi Ishikawa, MD, unpublished data, 1998).

In addition, each observer will set the reference point on any measurement in an idiosyncratic way. For example, when measuring corneal thickness, one observer may tend to select a reference point slightly more external on the epithelial surface than another observer. This situation would result in the first observer measuring greater corneal thickness, assuming that each observer would choose the same point as an endothelial border. In general, repeated measurement by the same observer is reasonably reproducible.

Quantitative measurement methods

Methods proposed by Pavlin and colleagues—Pavlin et al [1] established various quantitative measurement parameters as standards (Table 1, Fig. 15). The position of the scleral spur is used as a reference point for most of their parameters, because this is the only landmark that can be distinguished consistently in the anterior chamber angle region.

Iris concavity/convexity—Potash et al [24] introduced a parameter to evaluate the dynamic configurational change of the iris. A line is created from the most peripheral point to the most central point of iris pigment epithelium. A perpendicular line is then extended from this line to the iris pigment epithelium at the point of greatest concavity or convexity (Fig. 16).

An improved method for assessing the anterior chamber angle—There is one problem with AOD measurement, Pavlin's classical method of assessing the angle opening, which treats the iris surface as a straight line. Fig. 17 shows two schematics of the angle, demonstrating exactly the same value for the AOD and the trabecular–iris angle (TIA). Nevertheless, it is obvious that the angle on the right is gonioscopically narrower and more likely to be occludable than the angle on the left; therefore, irregularities of iris contour and curvature need to be taken into account. Ishikawa et al [25] defined the angle recess area (ARA) as the triangular area bordered by the anterior iris surface, corneal endothelium, and a line

perpendicular to the corneal endothelium drawn to the iris surface from a point 750 μm anterior to the scleral spur (Fig. 18). In this way, the iris irregularity is properly accounted for in the measurement.

The semi-automated software in the UBM Pro 2000 also calculates the ARA. After the observer selects the scleral spur, the program automatically processes the image, detects a border, and calculates the ARA. The program plots consecutive AODs from the base of the angle recess to 750 μm anterior to the scleral spur and performs linear regression analysis of consecutive AODs, producing two figures—the acceleration (or slope) and the y-intercept.

The acceleration describes how rapidly the angle is getting wider, using the tangent of the angle instead of degrees as the unit. In other words, the acceleration estimates the general shape of the angle, shallow or wide. The y-intercept refers to the distance between the scleral spur and the iris surface along the perpendicular to the trabecular meshwork plane. This generalized value describes the angle opening at the level of the scleral spur. Although these parameters may seem similar to the AOD and TIA, there is a fundamental difference between them. Because the acceleration and the y-intercept are purely mathematical calculations based on linear regression analysis of the consecutive AODs, they can be negative numbers, which is impossible for the physically measured AOD and TIA. A negative number for the acceleration means that the angle has an almost normal configuration at its peripheral part and becomes very shallow, or is attached to the cornea, at its central part (ie, appositional angle closure starting at Schwalbe's line with space remaining in the angle recess) (Fig. 19). A negative y-intercept means that the angle recess is very shallow or is attached to the cornea at its periphery, whereas it is relatively wide centrally (ie, plateau iris and synechial closure) (Fig. 20). By using three numerical values, the ARA, the acceleration, and the y-intercept, one can describe many types of angle configuration quantitatively.

Clinical application of quantitative ultrasound biomicroscopy analysis

Glaucoma—Anterior chamber angle parameters have been used in various studies, such as the development of the angle in normal infants and children in relation to age [26], the difference between angle-closure and normal eyes [27], and the iris convexity related to age [28]. Ishikawa et al [25] measured the ARA, acceleration, and y-intercept under standardized dark and light conditions and reported that the more posterior the iris insertion on the ciliary face, the less likely the provocative test would be positive. Esaki et al [29] found that the anterior chamber angle opening in normal Japanese eyes narrowed with age in a cross-sectional study.

Ultrasound biomicroscopy also provides a powerful tool to evaluate the effect of drug instillation on the anterior chamber angle, iris, and ciliary body. Kobayashi et al [30] found that the angle opening increased after the instillation of pilocarpine in eyes with narrow angles but decreased in eyes with a wider or normal angle. Marchini et al [31] reported that the potent mydriatic effect of 2% ibopamine was greater than that of 10% phenylephrine or 1% tropicamide.

Several studies have evaluated morphologic change after surgical procedures. Marraffa et al [32] found that loss of endothelial cells after laser iridotomy was inversely proportional to the distance of the iridotomy from the endothelium and scleral spur. Gazzard et al [33] reported that laser peripheral iridotomy produced changes in iris morphology that were different from those caused by an increase in illumination. Chiou et al [34] measured the time course of the size of collagen implants after deep sclerectomy. They quantitatively confirmed that the collagen implant dissolved slowly within 6 to 9 months, leaving a tunnel in the sclera.

Tumor—Ultrasound biomicroscopy is effective for the diagnosis and management of anterior segment tumors. Reminick et al [35] measured the size and extent of anterior segment tumors.

Marigo et al [36] described six eyes with anterior segment implantation cysts in a comparison of UBM images with size measurement with histopathologic findings.

Other situations—Other ocular diseases involving the anterior segment can be assessed using UBM. Avitabile et al [37] investigated the correlation between the thickness at the corneal apex and disease severity in eyes with keratoconus. Gentile et al [38] measured the ciliary body area in uveitic eyes. Maruyama et al [39] measured the height of ciliary detachment in eyes with Harada disease. Trindade et al [16] studied the relative position of the posterior chamber phakic intraocular lens. Intraocular lens–iris touch, intraocular lens–crystalline lens touch, and anterior chamber shallowing were observed after implantation.

Summary

Ultrasound biomicroscopy technology has become an indispensable tool in qualitative and quantitative assessment of the anterior segment. Advances in software design and algorithms will improve theoretical understanding of the pathophysiology of anterior segment disorders. Future applications of quantitative techniques will yield important information regarding mechanisms of angle closure, improving understanding of the dynamic functions of the iris, accommodation, presbyopia, and other aspects of anterior segment physiology and pathophysiology.

Acknowledgements

This article was supported in part by NIH contracts RO1-EY13178 and RO1-EY11289.

References

1. Pavlin CJ, Harasiewicz K, Foster FS. Ultrasound biomicroscopy of anterior segment structures in normal and glaucomatous eyes. Am J Ophthalmol 1992;113:381–9. [PubMed: 1558111]
2. Pavlin CJ, Sherar MD, Foster FS. Subsurface ultrasound microscopic imaging of the intact eye. Ophthalmology 1990;97:244–50. [PubMed: 2326015]
3. Pavlin CJ, Harasiewicz K, Sherar MD, et al. Clinical use of ultrasound biomicroscopy. Ophthalmology 1991;98:287–95. [PubMed: 2023747]
4. Tello C, Potash S, Liebmann J, et al. Soft contact lens modification of the ocular cup for high-resolution ultrasound biomicroscopy. Ophthalmic Surg 1993;24:563–4. [PubMed: 8043053]
5. Tello C, Liebmann JM, Ritch R. An improved coupling medium for ultrasound biomicroscopy. Ophthalmic Surg 1994;25:410–1. [PubMed: 8090428]
6. Ishikawa H, Inazumi K, Liebmann JM, et al. Inadvertent corneal indentation can cause artifactitious widening of the iridocorneal angle on ultrasound biomicroscopy. Ophthalmic Surg Lasers 2000;31:342–5. [PubMed: 10928676]
7. Potash SD, Tello C, Liebmann J, et al. Ultrasound biomicroscopy in pigment dispersion syndrome. Ophthalmology 1994;101:332–9. [PubMed: 8115154]
8. Breingan PJ, Esaki K, Ishikawa H, et al. Iridolenticular contact decreases following laser iridotomy for pigment dispersion syndrome. Arch Ophthalmol 1999;117:325–8. [PubMed: 10088809]
9. Roters S, Engels BF, Szurman P, et al. Typical ultrasound biomicroscopic findings seen in ocular hypotony. Ophthalmologica 2002;216:90–5. [PubMed: 11919432]
10. Berinstein DM, Gentile RC, Sidoti PA, et al. Ultrasound biomicroscopy in anterior ocular trauma. Ophthalmic Surg Lasers 1997;28:201–7. [PubMed: 9076793]
11. Park M, Kondo T. Ultrasound biomicroscopic findings in a case of cyclodialysis. Ophthalmologica 1998;212:194–7. [PubMed: 9562097]
12. Laroche D, Ishikawa H, Greenfield D, et al. Ultrasound biomicroscopic localization and evaluation of intraocular foreign bodies. Acta Ophthalmol Scand 1998;76:491–5. [PubMed: 9716340]

13. Sewelam A, Ismail AM, El Serogy H. Ultrasound biomicroscopy of haptic position after transscleral fixation of posterior chamber intraocular lenses. J Cataract Refract Surg 2001;27:1418–22. [PubMed: 11566525]
14. Manabe S, Oh H, Amino K, et al. Ultrasound biomicroscopic analysis of posterior chamber intraocular lenses with transscleral sulcus suture. Ophthalmology 2000;107:2172–8. [PubMed: 11097591]
15. Landau IM, Laurell CG. Ultrasound biomicroscopy examination of intraocular lens haptic position after phacoemulsification with continuous curvilinear capsulorhexis and extracapsular cataract extraction with linear capsulotomy. Acta Ophthalmol Scand 1999;77:394–6. [PubMed: 10463407]
16. Trindade F, Pereira F, Cronemberger S. Ultrasound biomicroscopic imaging of posterior chamber phakic intraocular lens. J Refract Surg 1998;14:497–503. [PubMed: 9791815]
17. Saragoussi JJ, Puech M, Assouline M, et al. Ultrasound biomicroscopy of Baikoff anterior chamber phakic intraocular lenses. J Refract Surg 1997;13:135–41. [PubMed: 9109069]
18. Maberly DA, Pavlin CJ, McGowan HD, et al. Ultrasound biomicroscopic imaging of the anterior aspect of peripheral choroidal melanomas. Am J Ophthalmol 1997;123:506–14. [PubMed: 9124247]
19. Pierro L, Conforto E, Resti AG, et al. High-frequency ultrasound biomicroscopy versus ultrasound and optical pachymetry for the measurement of corneal thickness. Ophthalmologica 1998;212(Suppl 1):1–3. [PubMed: 9730734]
20. Urbak SF. Ultrasound biomicroscopy. III. Accuracy and agreement of measurements. Acta Ophthalmol Scand 1999;77:293–7. [PubMed: 10406148]
21. Tello C, Liebmann J, Potash SD, et al. Measurement of ultrasound biomicroscopy images: intraobserver and interobserver reliability. Invest Ophthalmol Vis Sci 1994;35:3549–52. [PubMed: 8056531]
22. Urbak SF. Ultrasound biomicroscopy. I. Precision of measurements. Acta Ophthalmol Scand 1998;76:447–55. [PubMed: 9716332]
23. Urbak SF, Pedersen JK, Thorsen TT. Ultrasound biomicroscopy. II. Intraobserver and interobserver reproducibility of measurements. Acta Ophthalmol Scand 1998;76:546–9. [PubMed: 9826037]
24. Potash SD, Tello C, Liebmann J, et al. Ultrasound biomicroscopy in pigment dispersion syndrome. Ophthalmology 1994;101:332–9. [PubMed: 8115154]
25. Ishikawa H, Esaki K, Liebmann JM, et al. Ultrasound biomicroscopy dark room provocative testing: a quantitative method for estimating anterior chamber angle width. Jpn J Ophthalmol 1999;43:526–34. [PubMed: 10672884]
26. Kobayashi H, Ono H, Kiryu J, et al. Ultrasound biomicroscopic measurement of development of anterior chamber angle. Br J Ophthalmol 1999;83:559–62. [PubMed: 10216054]
27. Marchini G, Pagliarusco A, Toscano A, et al. Ultrasound biomicroscopic and conventional ultrasonographic study of ocular dimensions in primary angle-closure glaucoma. Ophthalmology 1998;105:2091–8. [PubMed: 9818611]
28. Ochiai H, Chihara E, Chuman H, et al. Age and increased incidence of “forward bowing” of the iris in normal eyes. J Glaucoma 1998;7:408–12. [PubMed: 9871863]
29. Esaki K, Ishikawa H, Liebmann JM, et al. Angle recess area decreases with age in normal Japanese. Jpn J Ophthalmol 2000;44:46–51. [PubMed: 10698025]
30. Kobayashi H, Kobayashi K, Kiryu J, et al. Pilocarpine induces an increase in the anterior chamber angular width in eyes with narrow angles. Br J Ophthalmol 1999;83:553–8. [PubMed: 10216053]
31. Marchini G, Babighian S, Tosi R, et al. Comparative study of the effects of 2% ibopamine, 10% phenylephrine, and 1% tropicamide on the anterior segment. Invest Ophthalmol Vis Sci 2003;44:281–9. [PubMed: 12506086]
32. Marraffa M, Marchini G, Pagliarusco A, et al. Ultrasound biomicroscopy and corneal endothelium in Nd: YAG-laser iridotomy. Ophthalmic Surg Lasers 1995;26:519–23. [PubMed: 8746572]
33. Gazzard G, Friedman DS, Devereux JG, et al. A prospective ultrasound biomicroscopy evaluation of changes in anterior segment morphology after laser iridotomy in Asian eyes. Ophthalmology 2003;110:630–8. [PubMed: 12623834]
34. Chiou AG, Mermoud A, Underdahl JP, et al. An ultrasound biomicroscopic study of eyes after deep sclerectomy with collagen implant. Ophthalmology 1998;105:746–50. [PubMed: 9544651]

35. Reminick LR, Finger PT, Ritch R, et al. Ultrasound biomicroscopy in the diagnosis and management of anterior segment tumors. J Am Optom Assoc 1998;69:575–82. [PubMed: 9785732]

36. Marigo FA, Finger PT, McCormick SA, et al. Anterior segment implantation cysts: ultrasound biomicroscopy with histopathologic correlation. Arch Ophthalmol 1998;116:1569–75. [PubMed: 9869783]

37. Avitabile T, Marano F, Castiglione F, et al. Keratoconus staging with ultrasound biomicroscopy. Ophthalmologica 1998;212(Suppl 1):10–2. [PubMed: 9730738]

38. Gentile RC, Liebmann JM, Tello C, et al. Ciliary body enlargement and cyst formation in uveitis. Br J Ophthalmol 1996;80:895–9. [PubMed: 8976700]

39. Maruyama Y, Kimura Y, Kishi S, et al. Serous detachment of the ciliary body in Harada disease. Am J Ophthalmol 1998;125:666–72. [PubMed: 9625550]

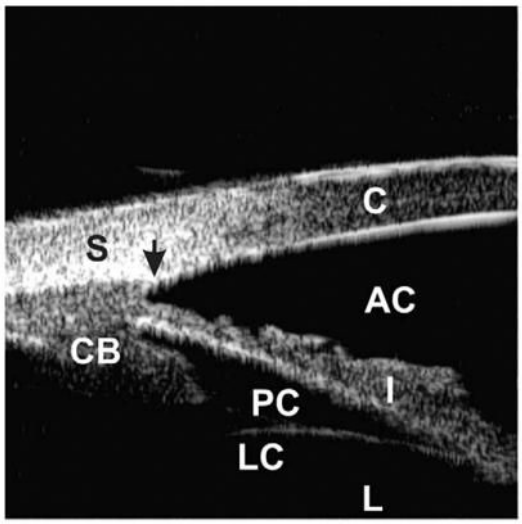

Fig 1.

Ultrasound biomicroscopic appearance of a normal eye. The cornea (C), sclera (S), anterior chamber (AC), posterior chamber (PC), iris (I), ciliary body (CB), lens capsule (LC), and lens (L) can be identified. The scleral spur (*black arrow*) is an important landmark to assess the morphologic relationships among the anterior segment structures.

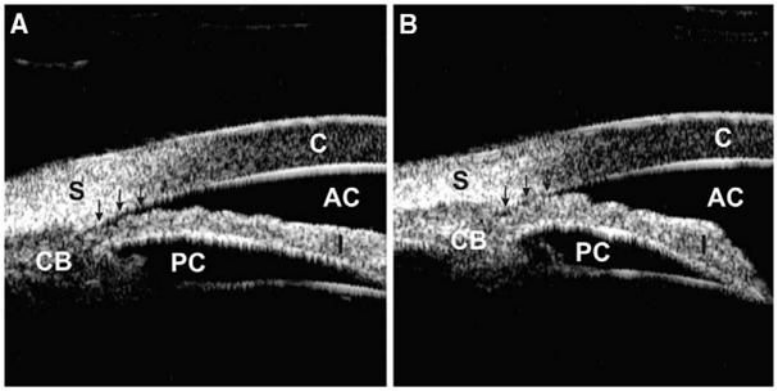

Fig 2.

Occludable angle with dark room provocative test. (*A*) The anterior chamber angle is slit-like opened (*arrows*) under a lighted condition. (*B*) The angle is completely occluded (*arrows*) under a dark condition.

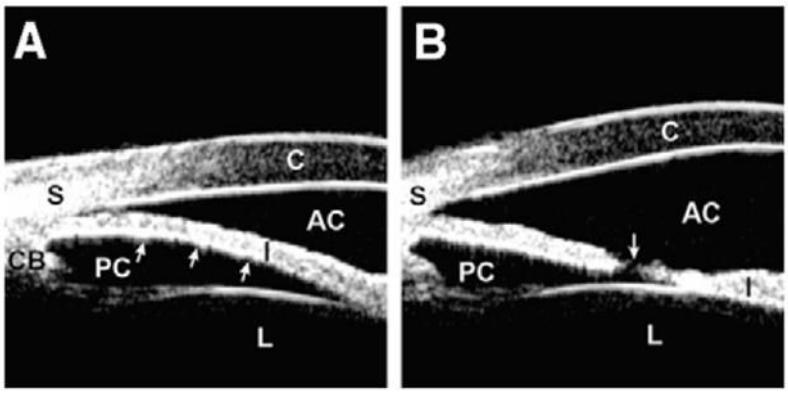

Fig 3.

Pupillary block. (*A*) The angle shows appositional closure owing to anterior bowing (*arrows*) of the iris. (*B*) The angle is open with a flattened iris after laser peripheral iridotomy. The patent hole on the iris (*arrow*) equalizes the pressure between the anterior and posterior chambers.

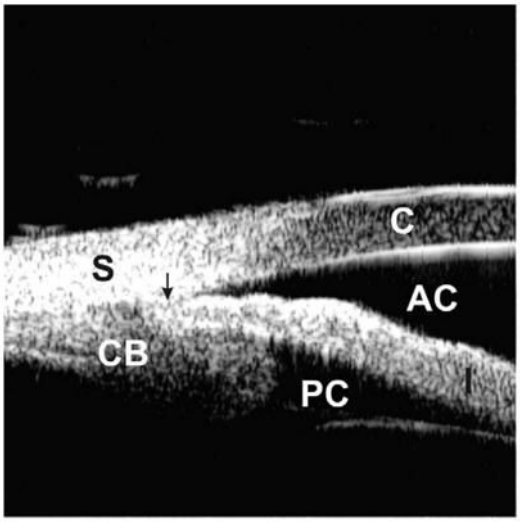

Fig 4.

Plateau iris. A large and anteriorly positioned ciliary body holds the iris root up against the cornea, leading to a partially occluded angle. The arrow represents the location of the scleral spur.

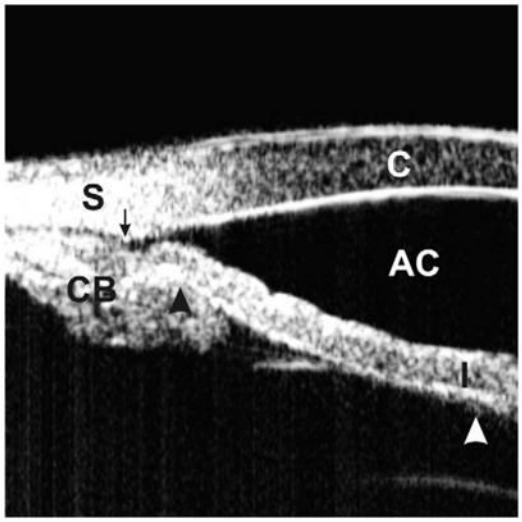

Fig 5.

Indentation UBM on an eye with a plateau iris. The angle is slit-like opened (the arrow represents the scleral spur location). The "double-hump" sign, one hump owing to the ciliary process (*black arrow head*) and the other owing to the lens (*white arrow head*), is demonstrated. (*Adapted from* Ishikawa H, Inazumi K, Liebmann JM, Ritch R. Inadvertant corneal indentation can cause artifactitious widening of the iridocorneal angle on ultrasound biomicroscopy. Ophthalmic Surg Lasers 2000;31(4):342 – 5; with permission.)

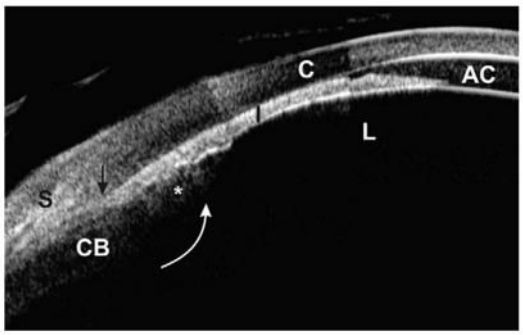

Fig 6.

Malignant glaucoma (composite image). The lens, iris, and ciliary process are all pushed forward, resulting in an extremely shallow anterior chamber and totally occluded angle. The ciliary process (*asterisk*) is completely anteriorly rotated (*white arrow*), probably pulled by zonules. The scleral spur is located at the black arrow.

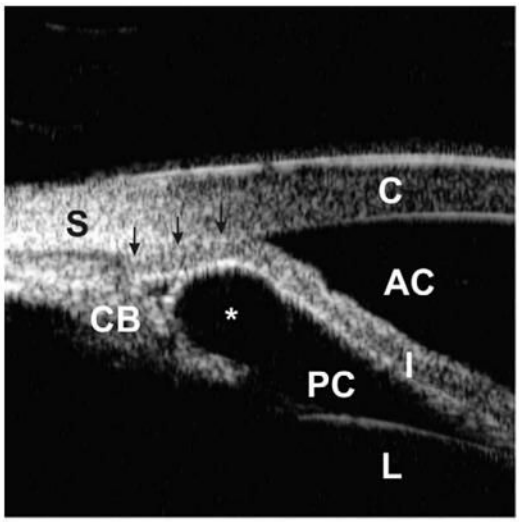

Fig 7.
Angle closure owing to an iridociliary cyst. An iridociliary cyst (*asterisk*) pushes the iris root toward the cornea, resulting in total occlusion of the angle (*arrows*).

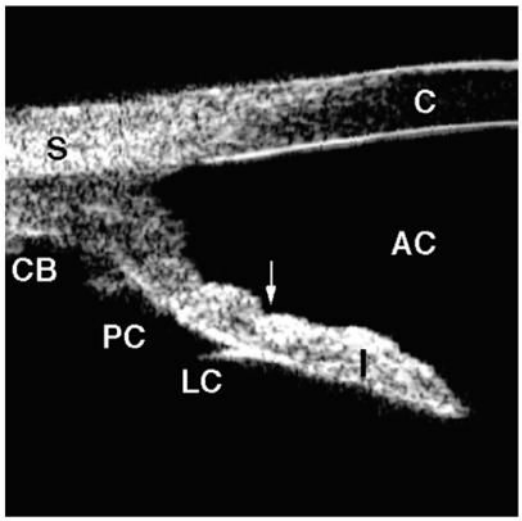

Fig 8.

Pigment dispersion syndrome. The angle is wide with a concave iris (*arrow*). Note the extremely wide iridolenticular contact. (*Adapted from* Breingan PJ, Esaki K, Ishikawa H, et al. Iridolenticular contact decreases following laser iridotomy for pigment dispersion syndrome. Arch Ophthalmol 1999;117(3):325–8; with permission.)

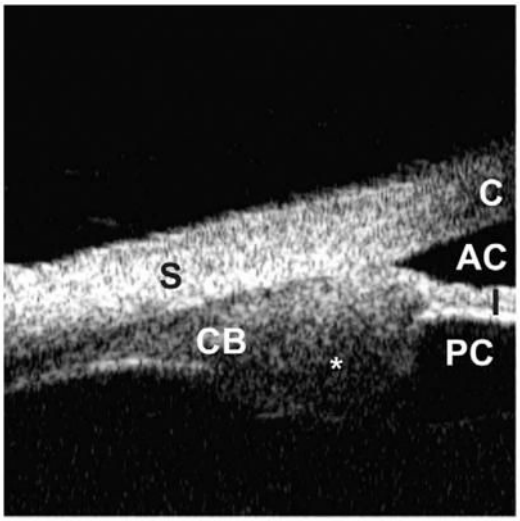

Fig 9.
Iridociliary tumor. Abnormally large ciliary process (*asterisk*) involving the iris root and pars plana is visualized.

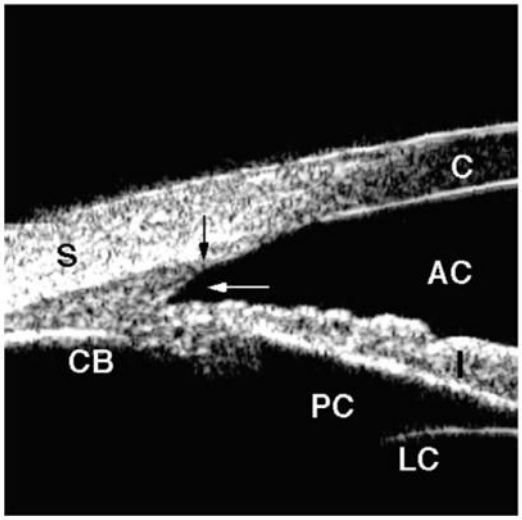

Fig 10.

Angle recession. Blunt trauma caused a tear into the ciliary body face (*white arrow*), but the iris remained attached to the scleral spur (*black arrow*). There is no direct communication between the anterior chamber and the supraciliary space.

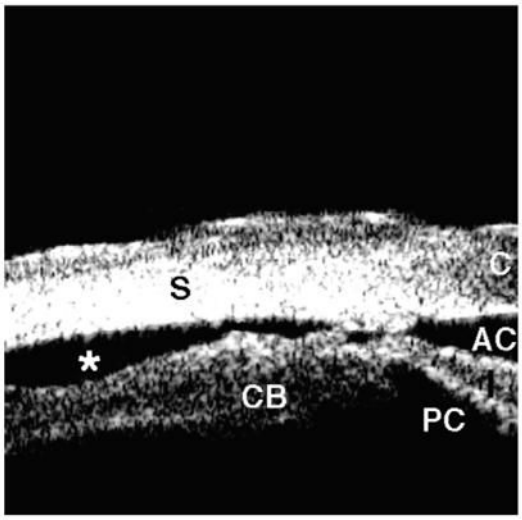

Fig 11.
Cyclodialysis. The ciliary body is avulsed from the sclera, resulting in free aqueous flow from the anterior chamber through the cleft into the supraciliary space (*asterisk*).

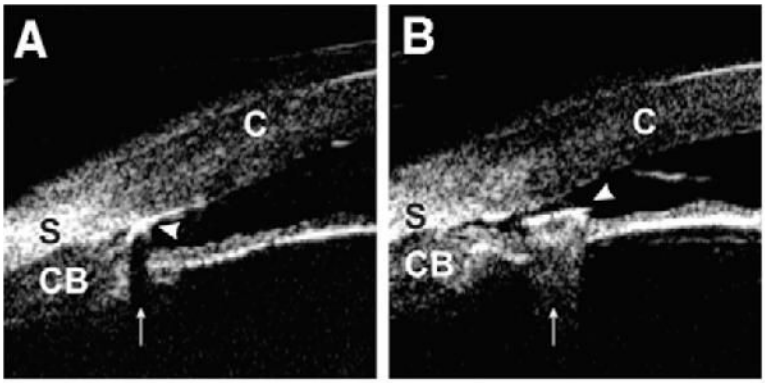

Fig 12.

Intraocular foreign body. (*A*) Foreign body (*arrow head*) with a material that consists of multiple cavities inside (ie, wood and concrete) generates shadowing artifact (*arrow*) by absorbing ultrasound power. The iris image is masked by shadowing. (*B*) Hard and dense foreign body (*arrow head*) (ie, glass and metal) creates comet tail artifact (*arrow*) owing to multiple internal reflections. The iris image is disrupted by the comet tail artifact. (*Adapted from* Laroche D, Ishikawa H, Greenfield D, et al. Ultrasound biomicroscopic localization and evaluation of intraocular foreign bodies. Acta Ophthalmol Scand 1998;76(4):491–5; with permission.)

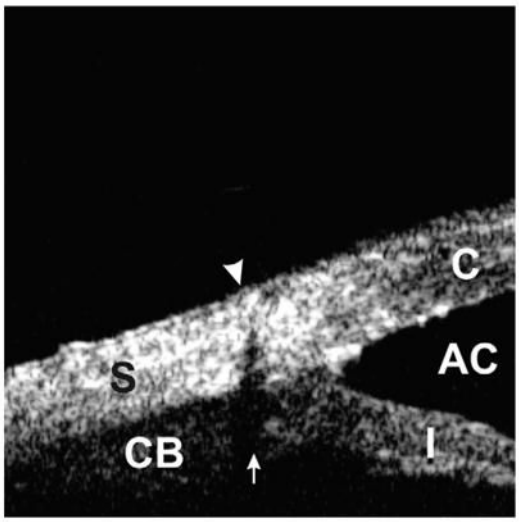

Fig 13.
Scleral suture can be identified by looking for its shadowing artifact (*arrow*). This artifact is created owing to refraction of the ultrasound beam at a boundary between suture thread and the surrounding tissues.

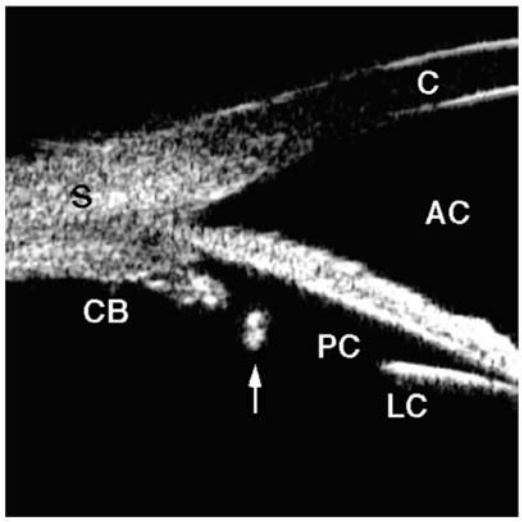

Fig 14.
Posterior chamber intraocular lens haptic. The most peripheral portion of the haptic is positioned within the capsular bag and is located central to the ciliary process (*arrow*).

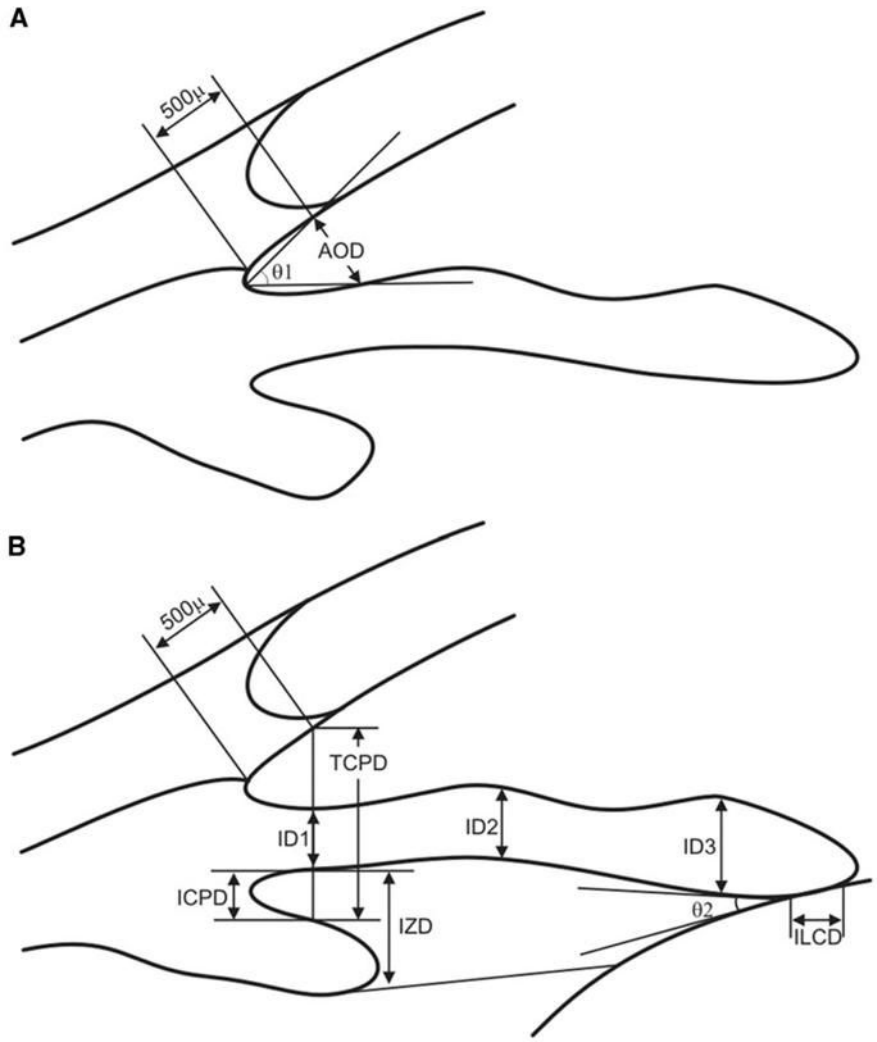

Fig 15.

Pavlin's measurement parameters (see Table 1). (*A*) The angle opening distance (AOD) is defined as the length of the line drawn from the point on the corneal endothelial surface 500 μm anterior to the scleral spur to the iris surface perpendicular to the corneal endothelial surface. The trabecular–iris angle (TIA, θ 1) is defined as an angle formed with the apex at the iris recess and the arms passing through the point on the meshwork 500 μm from the scleral spur and the point on the iris perpendicularly opposite. (*B*) The trabecular ciliary distance (TCPD) is defined as the distance between a point 500 μm from the scleral spur and the ciliary process on the line that is perpendicular through the iris. The iris thickness (ID1) is defined along this line, as is the iris–ciliary process distance (ICPD). Iris thickness also can be measured 2 mm from the iris root (ID2) and at its thickest point near the margin (ID3). The iris–zonule distance (IZD) is defined as a part of theTCPD at a point just clearing the ciliary process. The length of iris–lens contact (ILCD) and the angle at which the iris leaves the lens surface (iris–lens angle; ILA, θ 2) are easily measured.

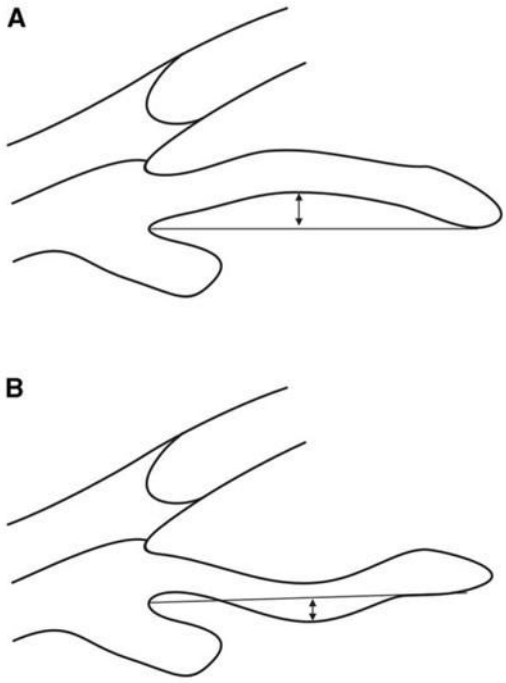

Fig 16.

Iris concavity/convexity. Iris configuration is determined first by creating a line from the most peripheral to the most central points of iris pigment epithelium. A perpendicular line is then extended from this line to the iris pigment epithelium at the point of greatest concavity or convexity. (*A*) Iris convexity measurement (*arrow*). (*B*) Iris concavity measurement (*arrow*).

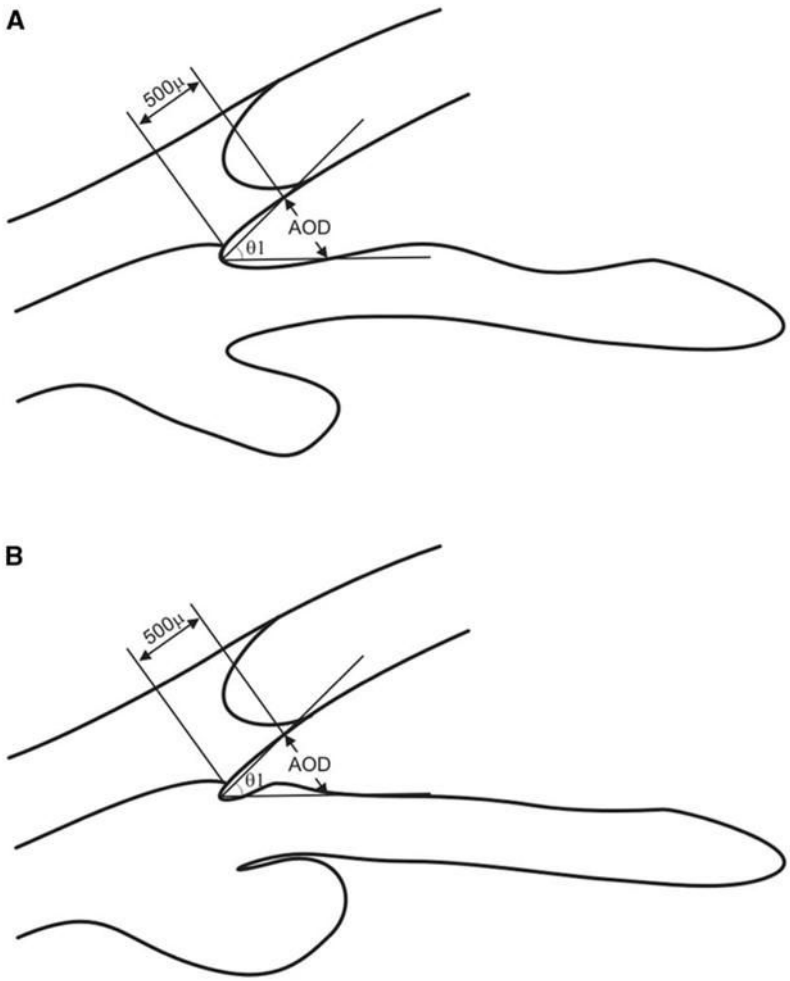

Fig 17.

Limitation of the conventional angle opening distance (AOD) measurement. (*A*) and (*B*) have exactly the same value for the AOD and trabecular–iris angle (TIA, θ 1). Nevertheless, the angle in (*B*) is gonioscopically narrower and is more likely to be occludable than the normal-appearing angle in (*A*).

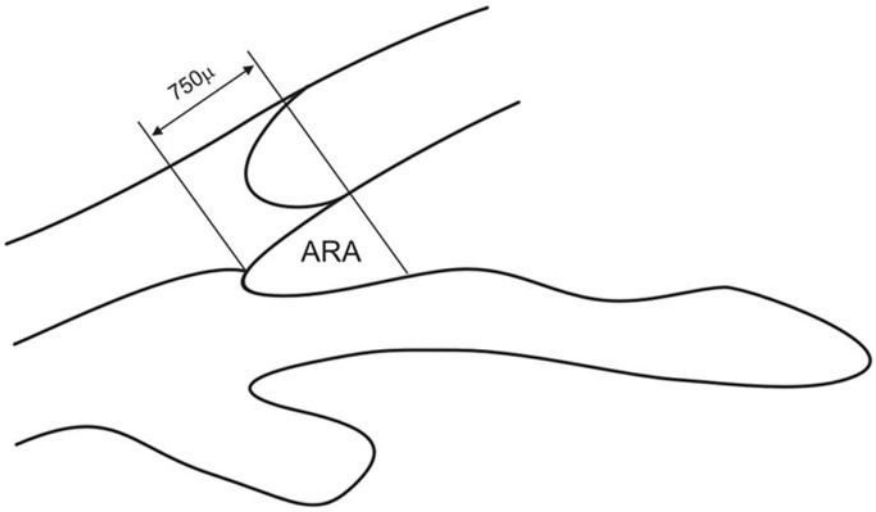

Fig 18.

Angle recess area (ARA). The ARA is defined as a triangular area bordered by the anterior iris surface, corneal endothelium, and a line perpendicular to the corneal endothelium drawn from a point 750 μm anterior to the scleral spur to the iris surface.

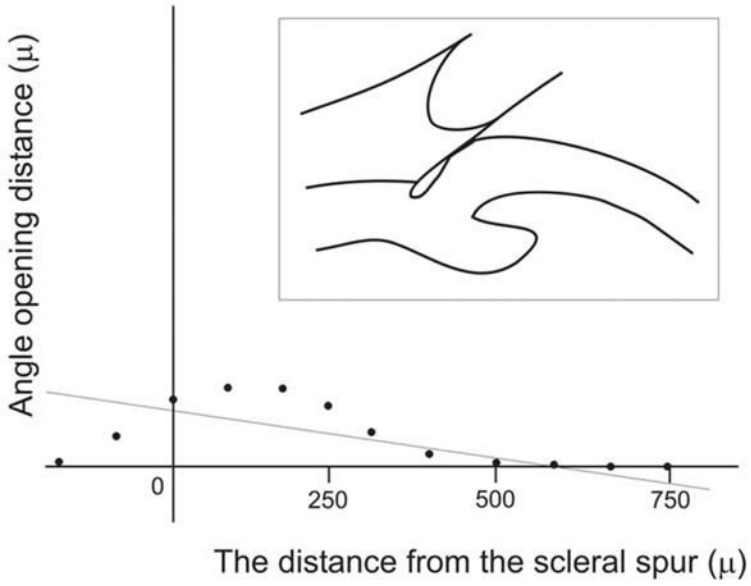

Fig 19.

Negative acceleration in ARA analysis. The linear regression analysis of ARA shows negative acceleration, meaning that the angle almost has a normal configuration at its peripheral part and becomes very shallow or is apposed to the cornea at its central part (ie, the appositional angle closure began at the level of Schwalbe's line).

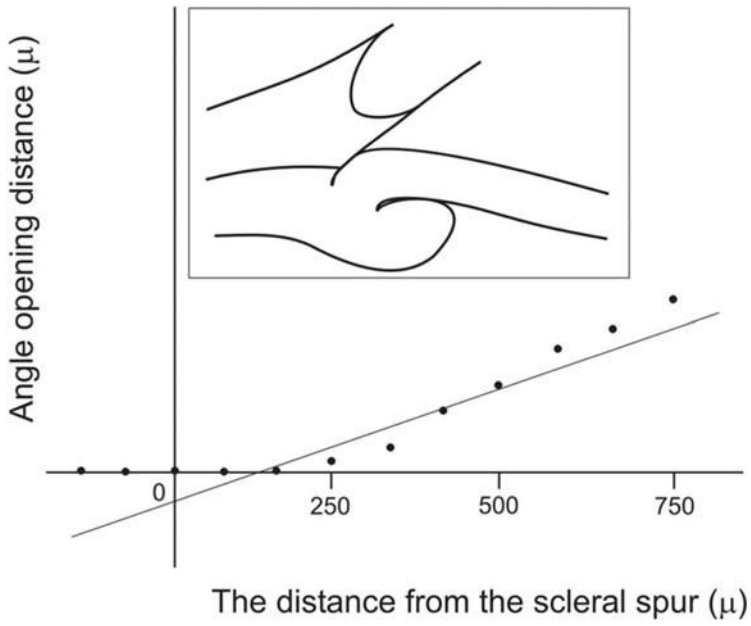

Fig 20.

Negative y-intercept in ARA analysis. The linear regression analysis shows a negative y-intercept, indicating that the angle recess is very shallow or is attached to the cornea at its periphery, whereas it has a relatively wide angle recess centrally (ie, plateau iris and synechial closure).

Table 1

Parameters proposed by Pavlin et al [1]

Name	Abbreviation	Description
Angle opening distance	AOD	Distance between the trabecular meshwork and the iris at 500 μm anterior to the scleral spur
Trabecular–iris angle	TIA θ 1	Angle of the angle recess
Trabecular–ciliary process distance	TCPD	Distance between the trabecular meshwork and the ciliary process at 500 μm anterior to the scleral spur
Iris thickness	ID1	Iris thickness at 500 μm anterior to the scleral spur
Iris thickness	ID2	Iris thickness at 2 mm from the iris root
Iris thickness	ID3	Maximum iris thickness near the pupillary edge
Iris–ciliary process distance	ICPD	Distance between the iris and the ciliary process along the line of TCPD
Iris–zonule distance	IZD	Distance between the iris and the zonule along the line of TCPD
Iris–lens contact distance	ILCD	Contact distance between the iris and the lens
Iris–lens angle	ILA θ 2	Angle between the iris and the lens near the pupillary edge